Electrically charged black holes in linear and nonlinear electrodynamics: Geodesic analysis and scalar absorption

Marco A. A. Paula,[1,*] Luiz C. S. Leite,[1,2,†] and Luís C. B. Crispino[1,‡]

[1]*Programa de Pós-Graduação em Física, Universidade Federal do Pará, 66075-110 Belém, Pará, Brazil*
[2]*Campus Altamira, Instituto Federal do Pará, 68377-630 Altamira, Pará, Brazil*

(Received 24 September 2020; accepted 27 October 2020; published 12 November 2020)

Along the last decades, several regular black hole (BH) solutions, i.e., singularity-free BHs, have been proposed and associated to nonlinear electrodynamics models minimally coupled to general relativity. Within this context, it is of interest to study how those nonlinear-electrodynamic-based regular BHs (RBHs) would interact with their astrophysical environment. We investigate the propagation of a massless test scalar field in the background of an electrically charged RBH solution, obtained by Eloy Ayón-Beato and Alberto García. Using a numerical approach, we compute the absorption cross section of the massless scalar field for arbitrary values of the frequency of the incident wave. We compare the absorption cross sections of the Ayón-Beato and García RBH with the Reissner-Nordström BH, showing that they can be very similar in the whole frequency regime.

DOI: 10.1103/PhysRevD.102.104033

I. INTRODUCTION

General relativity (GR) is a very well-established gravitational theory that has successfully passed through many experimental tests [1] and also predicted new astrophysical objects and phenomena, like black holes (BHs) [2] and gravitational waves [3]. Within GR, standard BHs are characterized by an event horizon and described by only three parameters, namely the following: the mass, the electric charge and the angular momentum [4]. However, despite this simplicity, the curvature singularities, hidden inside the BH event horizon according to the cosmic censorship conjecture [5], represent a potential challenge to GR.

During the last 50 years, many efforts have been made to circumvent the problem of intrinsic singularities within GR, including the so-called regular BH (RBH) solutions (for a review see, e.g., Ref. [6]). Historically, the first suggested RBHs lacked of a specified source associated to their line elements (see, e.g., Refs. [7–11] and references therein). However, in 1998, Eloy Ayón-Beato and Alberto García proposed a nonlinear electrodynamics (NED) model minimally coupled to GR [12] as a possible source to singularity-free charged BHs. The NED generalizes Maxwell's theory [13–15] and appears at certain energy levels of some string/M theories [16–18]. Based on a NED framework, several electrically [19–23] and magnetically [24–28] charged RBH solutions have been proposed, as well as NED-based RBH solutions in alternative theories of gravity [29,30].

It is well known that, in real astrophysical scenarios, BHs are surrounded by distributions of matter [31]. Within this context, in order to improve our understanding on BH physics, we can study how BHs absorb and scatter matter fields. Many investigations concerning the absorption and scattering have been made for standard BH solutions (see, e.g., Refs. [32–37] and references therein). Recently, some studies related to how test matter fields are absorbed and scattered by RBHs (in the NED framework) have also been carried out [38–41], but some features are yet to be investigated. For instance, in the scenarios of test scalar fields absorption, the role played by the RBH's electric charge and the possibility of such electrically charged RBHs mimic the standard BHs.

We study the absorption of a massless test scalar field in the background of the RBH solution obtained by Ayón-Beato and García (ABG) [12], which is a static, spherically symmetric, and electrically charged RBH. By using a numerical approach we compute the absorption cross section (ACS) for arbitrary values of the field frequency, and we also perform a classical analysis of the ACS. Noting that the ABG RBH has a causal structure similar to that of the Reissner-Nordström (RN) BH, we compare our results with the RN ones [42,43].

The remainder of this paper is organized as follows. In Sec. II we review the main aspects of the ABG RBH spacetime. We perform a classical analysis of the absorption of massless particles in Sec. III, and in Sec IV we study the dynamics of a massless scalar field in the background of the ABG RBH. In Sec. V we investigate the ACS using the

*marco.paula@icen.ufpa.br
†luiz.leite@ifpa.edu.br
‡crispino@ufpa.br

partial-wave method and exhibit approximations for the low- and high-frequency regime. In Sec. VI we present our main results associated to the ACS of the ABG RBH. We conclude with our final remarks in Sec. VII. Throughout this paper we use natural units, for which $G = c = \hbar = 1$, and the metric signature $(+,-,-,-)$.

II. ABG RBH SPACETIME

The NED theory (in the so-called P framework [25]) minimally coupled to GR can be described by the action

$$\mathrm{S} = \frac{1}{4\pi}\int d^4x\sqrt{-g}\left[\frac{1}{4}R - (2P\mathcal{H}_P - \mathcal{H}(P))\right], \quad (1)$$

where g is the determinant of the metric tensor $g^{\mu\nu}$, R is the corresponding Ricci scalar, $\mathcal{H}(P)$ is a Hamiltonian-like density quantity obtained through a Legendre transformation [44], and $\mathcal{H}_P \equiv \partial\mathcal{H}/\partial P$. The auxiliary antisymmetric tensor $P_{\mu\nu}$ and the scalar P are given by

$$P_{\mu\nu} = \mathcal{H}_P^{-1}F_{\mu\nu} \quad \text{and} \quad P \equiv \frac{1}{4}P_{\mu\nu}P^{\mu\nu}, \quad (2)$$

respectively, with $F_{\mu\nu}$ being the standard electromagnetic field strength. A correspondence with NED theory in the F framework can be obtained considering the following relations [44]:

$$\mathcal{L} = 2P\mathcal{H}_P - \mathcal{H}(P), \qquad \mathcal{L}_F\mathcal{H}_P = 1, \quad \text{and} \quad F = P\mathcal{H}_P^2, \quad (3)$$

in which $\mathcal{L}$ is a gauge-invariant electromagnetic Lagrangian density and $\mathcal{L}_F \equiv \partial\mathcal{L}/\partial F$, where F is the Maxwell scalar,

$$F = \frac{1}{4}F_{\mu\nu}F^{\mu\nu}. \quad (4)$$

For the RBH solution with mass M and electric charge Q obtained in Ref. [12], the corresponding NED source is determined by the function [12]

$$\mathcal{H}(P) = P\frac{(1-3\sqrt{-2Q^2P})}{(1+\sqrt{-2Q^2P})^3} - \frac{3M}{Q^3}\left(\frac{\sqrt{-2Q^2P}}{1+\sqrt{-2Q^2P}}\right)^{5/2}, \quad (5)$$

where the invariant P is a negative quantity.

In order to solve the Einstein-NED field equations obtained from the action (1), one may consider a static and spherically symmetric line element

$$ds^2 = f(r)dt^2 - \frac{1}{f(r)}dr^2 - r^2d\Omega^2, \quad (6)$$

where $d\Omega^2 = d\theta^2 + \sin^2\theta d\varphi^2$ is the line element of a unit 2-sphere, and also assume that

$$P_{\mu\nu} = (\delta^t_\mu\delta^r_\nu - \delta^t_\nu\delta^r_\mu)D(r). \quad (7)$$

It can be shown that $D(r) = Q/r^2$ and $P = -Q^2/2r^4$. Finally, one can show that the metric function $f(r)$ reads

$$f(r) = f^{\mathrm{ABG}}(r) \equiv 1 - \frac{2Mr^2}{(r^2+Q^2)^{3/2}} + \frac{Q^2r^2}{(r^2+Q^2)^2}. \quad (8)$$

In this paper we shall call a line element given by Eq. (6) with the metric function $f^{\mathrm{ABG}}(r)$ as the ABG line element, which has been originally obtained in Ref. [12].[1] We note that, as $r \to \infty$,

$$\lim_{r\to\infty} f^{\mathrm{ABG}}(r) \to f^{\mathrm{RN}}(r), \quad (9)$$

with

$$f^{\mathrm{RN}}(r) \equiv 1 - \frac{2M}{r} + \frac{Q^2_{\mathrm{RN}}}{r^2} \quad (10)$$

being the metric function of the RN spacetime.

Depending on the value of the ratio Q/M, the ABG RBH may possess up to two horizons, and their locations are given by

$$r_\pm \equiv |Q|\sqrt{\left(\pm\frac{\sqrt{z(s)}}{2\sqrt{6}s} + \frac{\sqrt{6u(s)+9}}{12s} + \frac{1}{4s}\right)^2 - 1}, \quad (11)$$

where we have used the auxiliary functions

$$z(s) \equiv -\frac{9(12s^2-1)}{\sqrt{6u(s)+9}} - u(s) - 12s^2 + 3, \quad (12)$$

$$u(s) \equiv -\frac{4(11s^2-3)s}{\sqrt[3]{4(w(s)+9s)}} + s\sqrt[3]{4(w(s)+9s)} - 4s^2, \quad (13)$$

and

$$w(s) \equiv 74s^3 + 3\sqrt{3}\sqrt{400s^6 - 112s^4 + 47s^2 - 4}, \quad (14)$$

in which $s \equiv |Q|/2M$. Here we shall restrict our analysis to BHs, which are described by the ABG line element if the condition $|Q| \le Q_{\mathrm{ext}} \approx 0.6341M$ is fulfilled [12]. When $|Q| < Q_{\mathrm{ext}}$ the ABG RBH possesses a Cauchy horizon at r_- and an event horizon at r_+, given by Eq. (11). For $|Q| = Q_{\mathrm{ext}}$ we have the so-called extreme ABG RBH, with $r_+ = r_-$, and $|Q| > Q_{\mathrm{ext}}$ leads to horizonless solutions. This causal structure is similar to the RN case, for which $Q^{\mathrm{RN}}_{\mathrm{ext}} = M$.

[1] We point out that Ayón-Beato and García also obtained other line elements in the NED context [19,20].

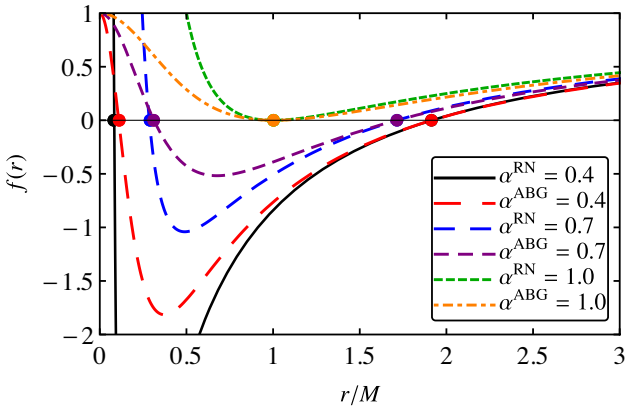

FIG. 1. Comparison between the metric functions of ABG and RN BHs, as a function of r, for different choices of the normalized charge. The colored circles represent the location of the horizons in each case.

In Fig. 1 we plot $f(r)$, both for ABG RBHs and for RN BHs, as a function of r, for different values of the normalized electric charge α, defined as

$$\alpha \equiv \frac{Q}{Q_{\rm ext}}. \tag{15}$$

For fixed values of α, we note that $f^{\rm ABG}(r) \to f^{\rm RN}(r)$ as $r \to \infty$, in accordance with Eq. (9). In Fig. 2 we plot the locations in which $f^{\rm ABG}(r) = f^{\rm RN}(r)$, as well as the horizons r_+ and r_- of ABG and RN BHs, for $0 \leq \alpha \leq 1$. We note that the horizons locations for both ABG and RN BH solutions, with a fixed α, are very similar. We also observe that the metric functions $f(r)$ of ABG and RN BHs may coincide at specific values of the radial coordinate r.

The (radial) electrostatic field $E(r)$ associated to the ABG solution is given by [12]

$$E^{\rm ABG}(r) = Qr^4\left(\frac{r^2-5Q^2}{(r^2+Q^2)^4} + \frac{15M}{2(r^2+Q^2)^{7/2}}\right), \tag{16}$$

which is finite at the origin (vanishing at $r = 0$) and behaves asymptotically as the electrostatic field in the RN case, namely

$$E^{\rm RN}(r) = \frac{Q_{\rm RN}}{r^2}, \tag{17}$$

as it is shown in Fig. 3. We also note that, near the BH center, $E^{\rm ABG}(r)$ decreases as we increase α, while the opposite behavior is observed for $E^{\rm RN}(r)$.

III. GEODESIC ANALYSIS

In this section we obtain the classical capture cross section, also known as the geometric cross section (GCS) of null geodesics. The classical (geometric) Lagrangian

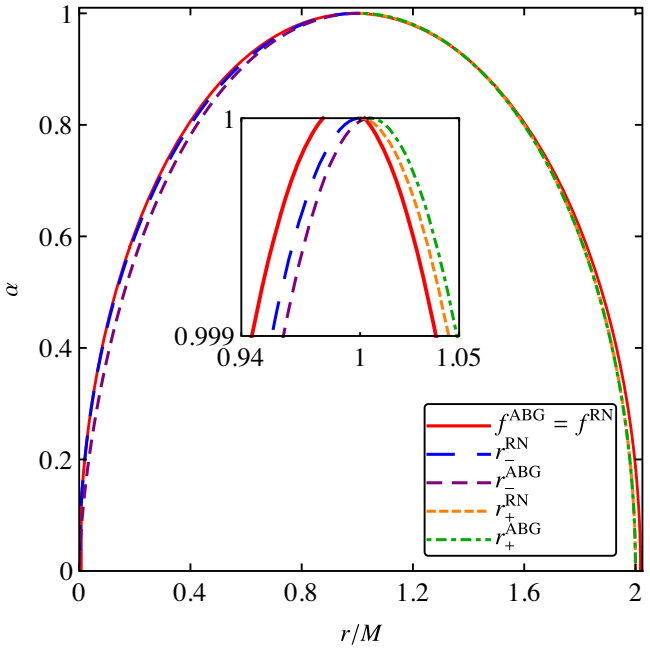

FIG. 2. The horizons of ABG and RN BHs for distinct choices of the normalized charge. We also plot the function $f^{\rm ABG}(r) = f^{\rm RN}(r)$. The central inset shows the plots near the extreme charge value. Notice that there is a discontinuity at $\alpha = 1$, for the plot $f^{\rm ABG}(r) = f^{\rm RN}(r)$.

related to the propagation of massless particles in the background of the line element (6) is given by

$$2{\rm L}_{\rm geo} = g_{\mu\nu}\dot{x}^\mu\dot{x}^\nu, \tag{18}$$

where the overdot denotes the derivative with respect to an affine parameter λ. Here, due to the spherical symmetry, we can consider, without loss of generality, the motion in the equatorial plane, i.e., $\theta = \pi/2$. We can then write

$${\rm L}_{\rm geo} = \frac{1}{2}\left(f(r)\dot{t}^2 - \frac{\dot{r}^2}{f(r)} - r^2\dot{\varphi}^2\right). \tag{19}$$

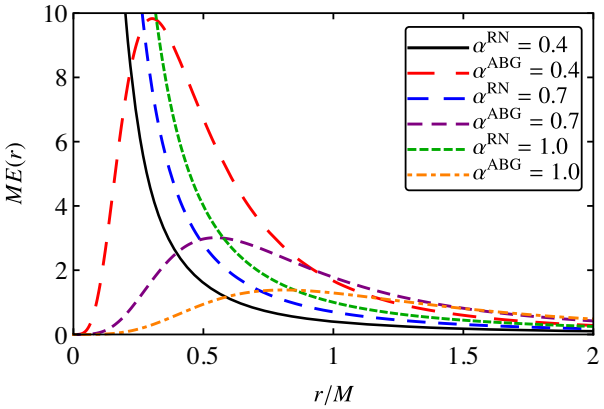

FIG. 3. The electrostatic fields of ABG and RN BHs, as a function of r, for different values of the normalized charge.

From Eq. (19), we note the existence of the following conserved quantities:

$$\frac{\partial \mathrm{L}_{\mathrm{geo}}}{\partial \dot{t}} = f(r)\dot{t} = E, \tag{20}$$

$$\frac{\partial \mathrm{L}_{\mathrm{geo}}}{\partial \dot{\varphi}} = -r^2\dot{\varphi} = -L, \tag{21}$$

where E and L are the energy and the angular momentum of a massless particle, respectively.

For null geodesics, the condition $\mathrm{L}_{\mathrm{geo}} = 0$ has to be satisfied. Using this condition together with Eqs. (20) and (21), and defining the impact parameter as

$$b \equiv \frac{L}{E}, \tag{22}$$

it is possible to obtain the following equation of motion:

$$\frac{\dot{r}^2}{L^2} = \mathrm{h}(r) \equiv \frac{1}{b^2} - \frac{f(r)}{r^2}. \tag{23}$$

From the conditions $\mathrm{h}(r)|_{r=r_c} = 0$ and $\frac{d\mathrm{h}(r)}{dr}|_{r=r_c} = 0$, we get the following pair of equations

$$2f(r_c) - r_c f'(r_c) = 0, \tag{24}$$

$$b_c = \frac{L_c}{E_c} = \frac{r_c}{\sqrt{f(r_c)}}, \tag{25}$$

where the prime symbol, $'$, denotes the derivative with respect to the radial coordinate r. Using Eqs. (24) and (25), it is possible to find the critical radius, r_c, and the critical impact parameter, b_c, that is, the radius of an unstable circular orbit and the value for the ratio L/E in the corresponding circular orbit, respectively. By solving Eq. (24) numerically we can compute r_c for a given α and consequently find b_c. Since the GCS of null geodesics is given by $\sigma_{\mathrm{geo}} = \pi b_c^2$ [5], we obtain

$$\sigma_{\mathrm{geo}} = \pi \frac{r_c^2}{f(r_c)}. \tag{26}$$

In Fig. 4 we show r_c and b_c for ABG and RN BHs, as functions of α. We note that, for a fixed value of α, $r_c^{\mathrm{ABG}} > r_c^{\mathrm{RN}}$ and $b_c^{\mathrm{ABG}} > b_c^{\mathrm{RN}}$, except in the chargeless case ($\alpha = 0$), for which both results tend to the Schwarzschild values, namely $r_c = 3M$ and $b_c = 3\sqrt{3}M$. As a consequence of the behavior presented by the critical value of the impact parameter, b_c, the GCS of the ABG RBH is larger than the corresponding RN BH one.

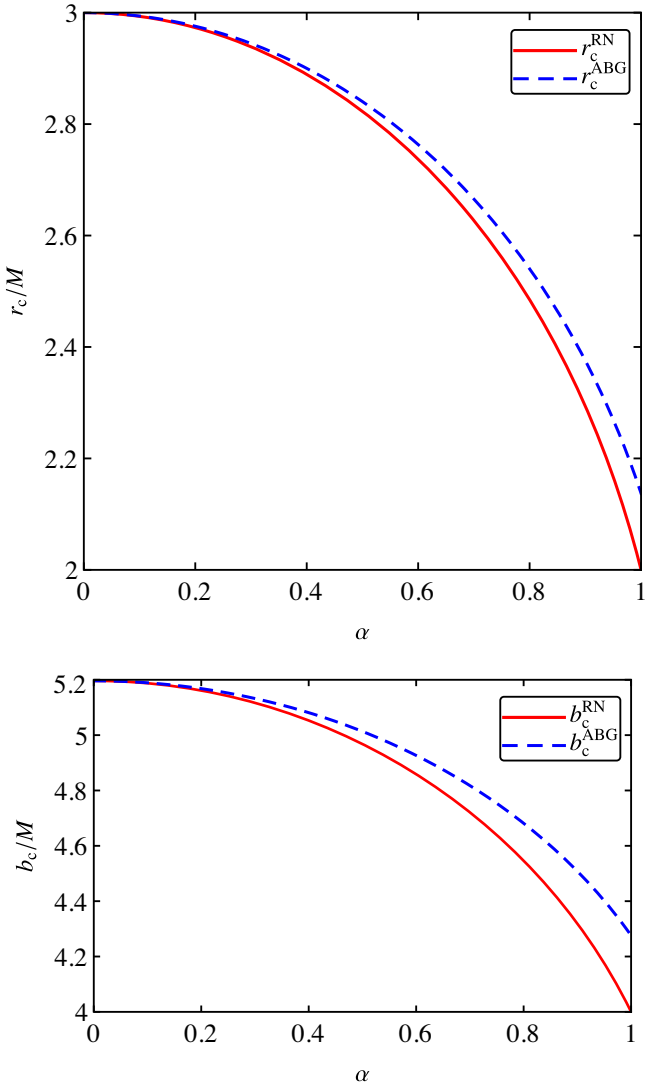

FIG. 4. The critical radius (top panel) and the critical impact parameter (bottom panel) of ABG and RN BHs as functions of the normalized charge.

IV. SCALAR FIELD

The dynamics of a massless and chargeless test scalar field Φ is governed by the Klein-Gordon equation, i.e.,

$$\nabla_\mu \nabla^\mu \Phi = \frac{1}{\sqrt{-g}} \partial_\mu (\sqrt{-g} g^{\mu\nu} \partial_\nu) \Phi = 0. \tag{27}$$

Considering the spherical symmetry of the spacetime under consideration, we can decompose Φ as

$$\Phi \equiv \sum_l^\infty C_{\omega l} \Phi_{\omega l} = \sum_l^\infty C_{\omega l} \frac{\Psi_{\omega l}(r)}{r} P_l(\cos\theta) e^{-i\omega t}, \tag{28}$$

where $\Psi_{\omega l}(r)$ is a radial function and $P_l(\cos\theta)$ is the Legendre polynomial. The constant coefficients $C_{\omega l}$ will be determined by the boundary conditions, and the indexes

ω and l denote the frequency and the angular momentum of the plane wave, respectively. By inserting Eq. (28) in Eq. (27) and defining the tortoise coordinate, $r_\star$, as

$$\frac{dr_\star}{dr} \equiv \frac{1}{f(r)}, \tag{29}$$

we get the following radial equation for $\Psi_{\omega l}(r)$

$$\frac{d^2}{dr_\star^2}\Psi_{\omega l} + (\omega^2 - V_{\rm eff}(r))\Psi_{\omega l} = 0, \tag{30}$$

in which the effective potential $V_{\rm eff}$ reads

$$V_{\rm eff}(r) = f(r)\left[\frac{1}{r}\frac{df(r)}{dr} + \frac{l(l+1)}{r^2}\right]. \tag{31}$$

We note that the domain of the tortoise coordinate is $(-\infty, \infty)$, whereas the domain of the coordinate r is $[r_+, \infty)$. In Fig. 5 we present $V_{\rm eff}(r)$ as a function of the radial coordinate, for different choices of l and α. We note that $V_{\rm eff}^{\rm ABG}(r)$ has a peak close to r_+, which increases as we increase the values of l or α. Besides that, $V_{\rm eff}(r)$ vanishes in the asymptotic limits, i.e.,

$$\lim_{r_\star \to \pm\infty} V_{\rm eff}(r_\star) = 0. \tag{32}$$

For the absorption/scattering problem under analysis, we consider plane waves incoming from the infinite null past (the so-called *in modes*). Therefore, we are interested in solutions of Eq. (30) subjected to the following boundary conditions

$$\Psi_{\omega l} \sim \begin{cases} T_{\omega l} e^{-i\omega r_\star}, & r \to r_+ (r_\star \to -\infty), \\ e^{-i\omega r_\star} + R_{\omega l} e^{i\omega r_\star}, & r \to \infty (r_\star \to \infty), \end{cases} \tag{33}$$

where $|T_{\omega l}|^2$ and $|R_{\omega l}|^2$ are the transmission and reflection coefficients, respectively. The plane wave subjected to the boundary conditions (33) comes from infinity, interacts with the effective potential (31), being partially transmitted into the BH and partially reflected back to infinity. Moreover, by using the conservation of the flux, it is possible to show that the quantities $R_{\omega l}$ and $T_{\omega l}$ satisfy

$$|R_{\omega l}|^2 + |T_{\omega l}|^2 = 1. \tag{34}$$

V. ABSORPTION CROSS SECTION

A. Partial-waves approach

In a BH absorption/scattering problem associated to static and spherically symmetric spacetimes, we consider that the field Φ behaves far from the BH as

$$\Phi \sim \Phi^{(\rm plane)} + \Phi^{\rm S}, \tag{35}$$

where $\Phi^{(\rm plane)}$ is a monochromatic planar wave propagating along the z axis, given by

$$\Phi^{(\rm plane)} = e^{-i\omega(t-z)}, \tag{36}$$

and $\Phi^{\rm S}$ is an outgoing scattered wave, i.e.,

$$\Phi^{\rm S} = \frac{1}{r}\hat{f}(\theta)e^{-i\omega(t-r)}, \tag{37}$$

in which $\hat{f}(\theta)$ is the scattering amplitude. We can decompose $e^{i\omega z}$ as [32]

$$e^{i\omega z} = \sum_{l=0}^{\infty}(2l+1)i^l j_l(\omega r)P_l(\cos\theta), \tag{38}$$

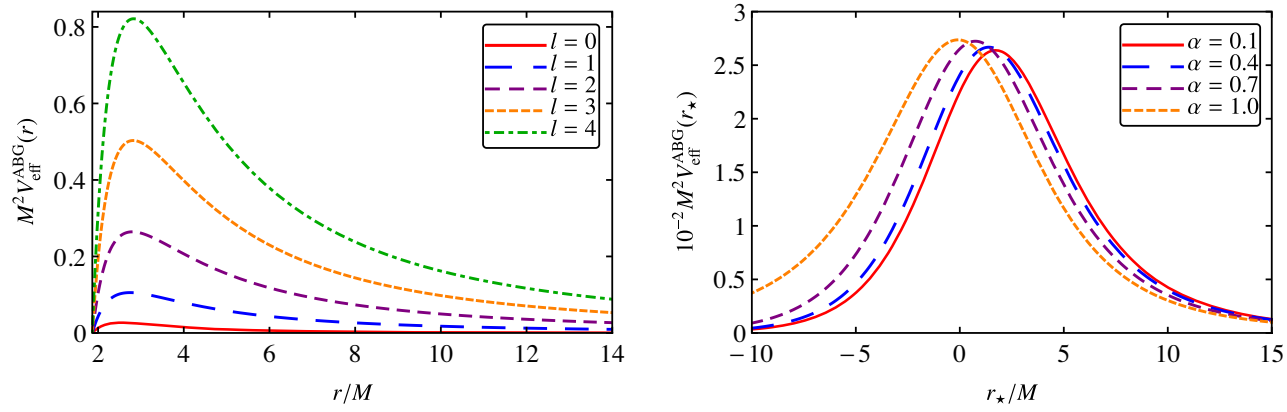

FIG. 5. The effective potential of massless and chargeless scalar waves in the background of the ABG RBH: (i) as a function of r for different choices of l, with $\alpha = 0.5$ (left panel); and (ii) as a function of $r_\star$ with $l = 0$, for different choices of the normalized charge (right panel).

with $j_l(\cdot)$ being the spherical Bessel function. In the far field region ($r \to \infty$), we can write

$$\Phi^{(\text{plane})} \sim \frac{e^{-i\omega t}}{r} \sum_{l=0}^{\infty} B_{\omega l}(e^{-i\omega r} + e^{-i\pi(l+1)} e^{i\omega r}) \times P_l(\cos\theta), \tag{39}$$

where

$$B_{\omega l} = \frac{(2l+1)}{2i\omega} e^{i\pi(l+1)}. \tag{40}$$

If we choose a boundary condition such that the ingoing part of Eq. (28) resembles, in the far field, the ingoing part of Eq. (35), it follows that $C_{\omega l} = B_{\omega l}$. Thus we get

$$\Phi = \sum_{l=0}^{\infty} B_{\omega l} \Phi_{\omega l}. \tag{41}$$

The ACS is related to the flux of particles transmitted into the BH. Accordingly, an expression for the ACS can be obtained by introducing the four-current density vector

$$J^{\mu} = \frac{i}{2}(\Phi^* \nabla^{\mu} \Phi - \Phi \nabla^{\mu} \Phi^*), \tag{42}$$

which satisfies the conservation law $\nabla_{\mu} J^{\mu} = 0$ associated to the Klein-Gordon equation (27). By inserting $\Phi_{\omega l}$ presented in Eq. (28), with $\Psi_{\omega l}$ given by Eq. (33) in the corresponding asymptotic limit, into Eq. (41) and using the orthogonality of the Legendre polynomials, i.e.,

$$\int P_l(\cos\theta) P_n(\cos\theta) d\Omega = \frac{4\pi}{2l+1} \delta_{ln}, \tag{43}$$

the surface integral of the current density vector (42) leads to

$$N(r) = -\int_{\Sigma} r^2 J^r \mathrm{d}\Omega = -\frac{\pi}{\omega} \sum_{l=0}^{\infty} (2l+1)(1 - |R_{\omega l}|^2), \tag{44}$$

which is the flux passing thought a surface Σ of constant radius r. If we consider stationary scenarios, this flux will be constant and N will be (minus) the number of particles absorbed by the BH per unit of time [45].

The total ACS, $\sigma(\omega)$, is defined as the ratio between the flux of Φ that goes into the BH, $|N|$, and the current of the incident planar wave, $J^z_{\text{inc}} = \omega$; so that we may write

$$\sigma(\omega) \equiv \frac{|N|}{J^z_{\text{inc}}} = \sum_{l=0}^{\infty} \sigma_l(\omega), \tag{45}$$

where the partial ACS, $\sigma_l(\omega)$, reads

$$\sigma_l(\omega) = \frac{\pi}{\omega^2}(2l+1)(1 - |R_{\omega l}|^2). \tag{46}$$

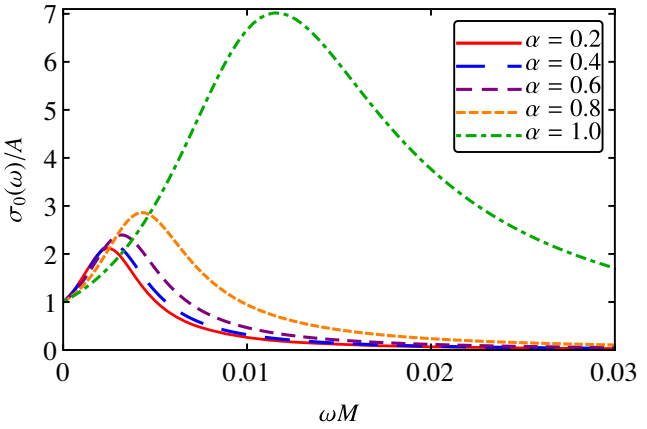

FIG. 6. The ACS of the ABG RBH for a massless chargeless scalar field divided by its area, as a function of ω, considering the monopole mode ($l = 0$) and different values of the normalized charge.

B. Low- and high-frequency regimes

In the low-frequency regime, it has been shown that, for stationary BH solutions, the ACS tends to the surface area of the BH event horizon [46,47], which is given by

$$A = 4\pi r_+^2. \tag{47}$$

In Fig. 6 we show the partial ACS of the $l = 0$ mode, $\sigma_0(\omega)$, divided by the BH area, as a function of the coupling ωM. We see that, as $\omega \to 0$, the ratio $\sigma_0(\omega)/A$ tends to the unity, showing that, at the zero-frequency limit, the numerical result for the ACS tends to the BH area, as expected. This result can also be regarded as a consistency check of our numerical results.

In Fig. 7 we compare the surface area of the BH event horizon of ABG, Bardeen and RN BHs, as functions of α. The high similarity between the value of r_+ (cf. Sec. II and, in particular, Fig. 2) for ABG and for RN BHs, for the same value of α, implies in very similar BH areas for the two cases. We also note that, for a fixed α, the areas of ABG and RN BHs are smaller than Bardeen one.[2]

In the high-frequency regime, massless and chargeless scalar waves can be described by null geodesics. Therefore, in this limit, the absorption of a massless scalar field is governed by Eq. (26). An improvement of the high-frequency approximation for the ACS is obtained by the so-called sinc approximation, which reveals the oscillatory behavior of the ACS. Within this approximation, the ACS can be expressed as [48,49]

[2]We take the opportunity to mention that in the caption of Fig. 10 of Ref. [38] the sentence "We have chosen $(Q_{\text{RN}}, Q_{\text{BD}})$ to be (0.6, 0.46809) and (0.8, 0.63252)" should be replaced by "We have chosen $(Q_{\text{RN}}, Q_{\text{BD}})$ to be (0.46809,0.6) and (0.63252,0.8)." A similar correction is in order in the corresponding part of the text of Ref. [38] in which Fig. 10 is explained.

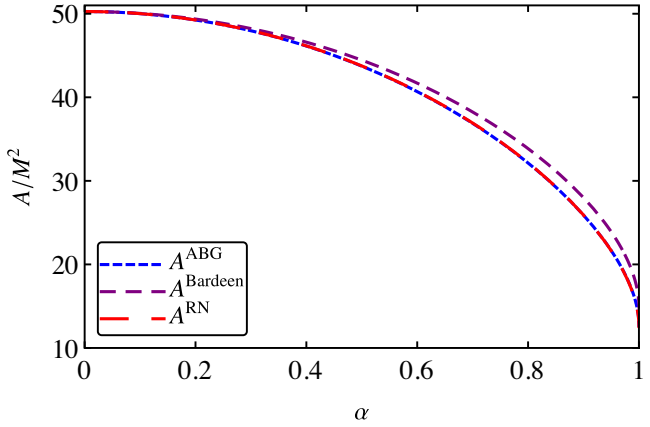

FIG. 7. The horizon area of ABG, Bardeen and RN BHs as a function of the normalized charge.

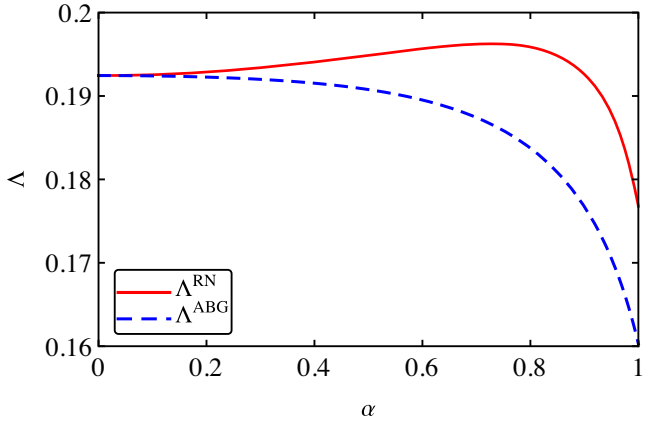

FIG. 8. The Lyapunov exponent of ABG and RN BHs, as functions of the normalized charged.

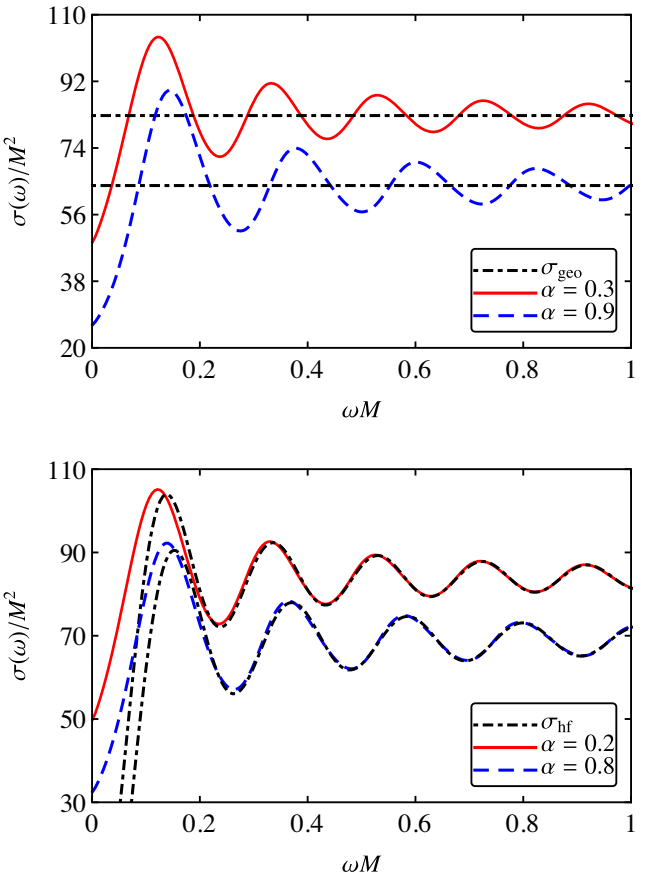

FIG. 9. The total ACS of the ABG RBH for different values of the normalized charge as a function of ω. In the top panel we exhibit the corresponding GCSs (horizontal dot-dashed lines), while in the bottom panel we exhibit the corresponding sinc approximation (dot-dashed lines).

$$\sigma_{\rm hf} = \sigma_{\rm geo}[1 - 8\pi b_c \Lambda e^{-\pi b_c \Lambda} \mathrm{sinc}(2\pi b_c \omega)], \quad (48)$$

where $\mathrm{sinc}(x) \equiv \sin(x)/x$, and Λ is the Lyapunov exponent related to the unstable circular orbit [50], which is given by

$$\Lambda = \sqrt{\frac{L_c^2}{2\dot{t}^2}\left(\frac{d^2\mathrm{h}(r)}{dr^2}\right)\Big|_{r=r_c}}. \quad (49)$$

The Eq. (48) is known as the sinc approximation to the ACS. In Fig. 8 we compare Lyapunov exponent Λ of ABG and RN BHs. We see that $\Lambda^{\rm ABG}$ is smaller than $\Lambda^{\rm RN}$, tending to the same value as $\alpha \to 0$, i.e., in the Schwarzschild BH limit. We show some results obtained using the sinc approximation in our numerical analysis in Sec. VI A.

C. Numerical analysis

We integrate numerically Eq. (30) from very close to the BH event horizon r_+, up to some radial position very far from the BH, typically chosen as $r_\infty \sim 10^3 M$. The appropriate boundary conditions close to the r_+ and in the far field are given by Eq. (33).

With the numerical results obtained for the reflection and transmission coefficients of the scalar wave, the ACS can be computed for arbitrary values of the frequency coupling ωM. For the results presented in this paper, in general, we have performed the summations in the angular momentum up to $l = 10$. The GCS and the sinc approximation are obtained using Eqs. (26) and (48), respectively. A selection of our numerical results is presented in Sec. VI. We have chosen to scale the ACS with the BH mass.

VI. RESULTS

A. Absorption by the ABG RBH: Main features

In Figs. 9 and 10 we plot the total ACS of the ABG RBH for different values of α as a function of the frequency coupling ωM. We note that the from mid-to-high values of the frequency the total ACS typically oscillates around the corresponding GCS (cf. top panel of Fig. 9). We also observe that the sinc approximation gives an excellent

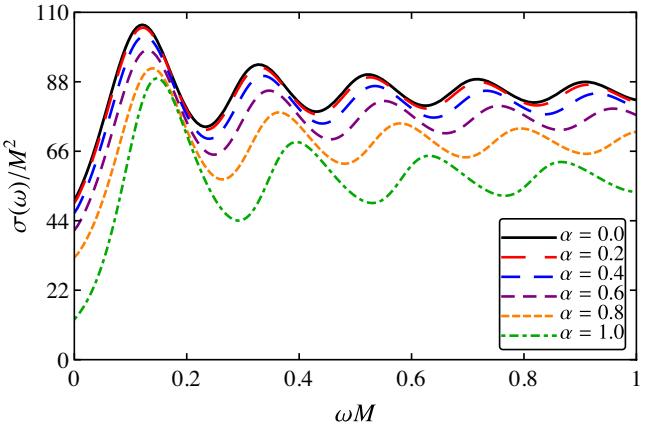

FIG. 10. The total ACS of the ABG RBH for different values of normalized charge as a function of ω.

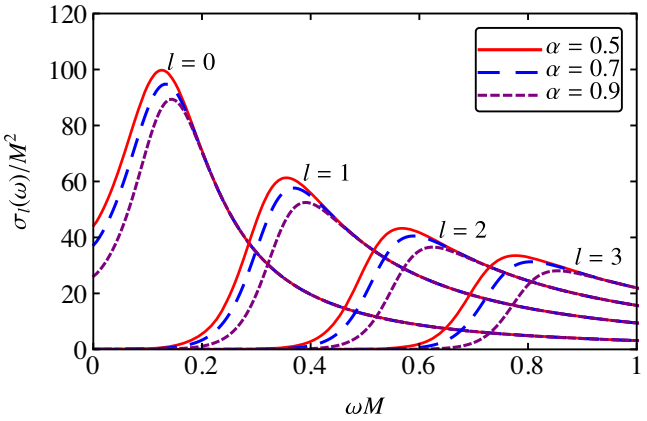

FIG. 11. The partial ACS of the ABG RBH for different values of normalized charge as a function of ω.

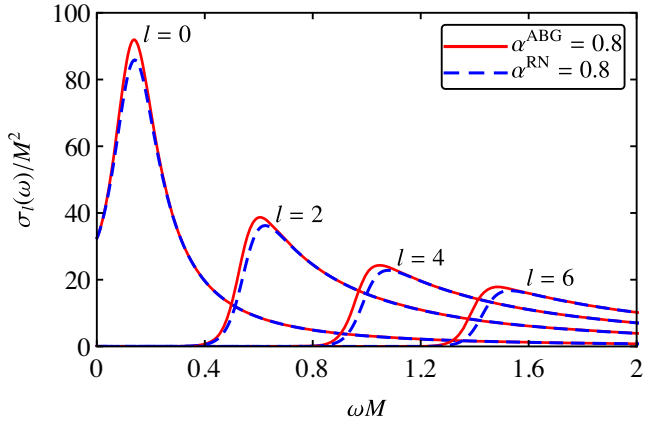

FIG. 12. The partial ACSs of ABG and RN BHs for different values of normalized charge as a function of ω.

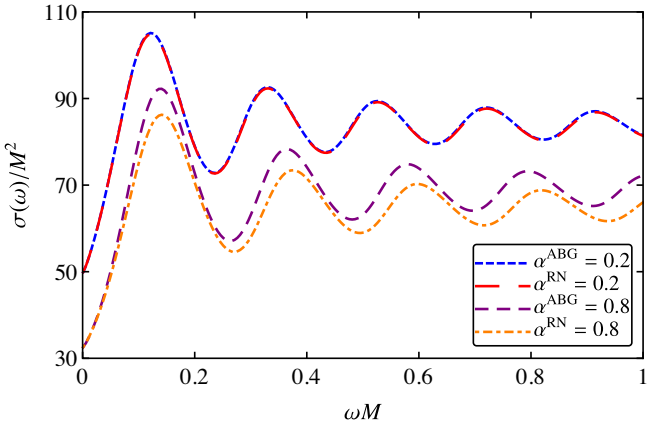

FIG. 13. The total ACSs of ABG and RN BHs for two selected values of the normalized charge as a function of ω.

approximation for the total ACS in this frequency regime (cf. bottom panel of Fig. 9). We also note that the total ACS of the ABG RBH decreases as we increase α (cf. Fig. 10).

In Fig. 11 we show the partial ACS of ABG RBHs for different choices of α as a function of ω. As we can see, the partial-waves modes present a peak, which decreases as we increase α, and vanish in the limit $\omega M \to \infty$. Moreover, for a fixed value of α, the maximum of the partial ACS of the ABG RBH is bigger than in the corresponding RN BH case, as it is shown in Fig. 12.

In Fig. 13 we present a comparison of the total ACS of ABG RBHs with the corresponding RN BHs with the same values of α as a function of ω. For small values of α, the total ACS of both BH solutions can be very similar along the whole frequency range. Nevertheless, as we increase α, we note that the total ACS of the ABG RBH is typically larger than the corresponding RN case. The ACSs of ABG and RN BHs, for the same choice of α, have very similar low-frequency values, in accordance with the fact that the areas of ABG and RN BHs with the same α are very similar (cf. Sec. V B and, in particular, Fig. 7).

B. Can RBHs mimic standard BHs?

We have seen that for low values of the normalized charge, the results for the ACS of ABG BHs are similar to those of RN BHs, in the whole frequency range. This similarity opens up the possibility of RBHs mimic standard BHs solutions, when one considers the absorption results by charged BHs. We can thus search for certain values for the pair $(\alpha^{ABG}, \alpha^{RN})$ to find situations in which the results for the ACSs are similar in the whole frequency range. A good starting point are the values of $(\alpha^{ABG}, \alpha^{RN})$ for which the GCSs coincide. From Fig. 14 we notice that the equality between the GCSs of ABG and RN BHs can be found up to $(\alpha^{ABG}, \alpha^{RN}) = (1, 0.9161)$. We then compute the ACSs for such values, in the whole frequency regime.

In Fig. 15 we exhibit the total ACSs for some pairs $(\alpha^{ABG}, \alpha^{RN})$, for which the GCSs are the same. For low to moderate values of the normalized charge α, we observe that the total ACS of the ABG and RN BHs can be very similar for arbitrary values of the wave frequency. However, for higher values of α, we see that the ACSs start to differ, specially in the low-frequency regime.

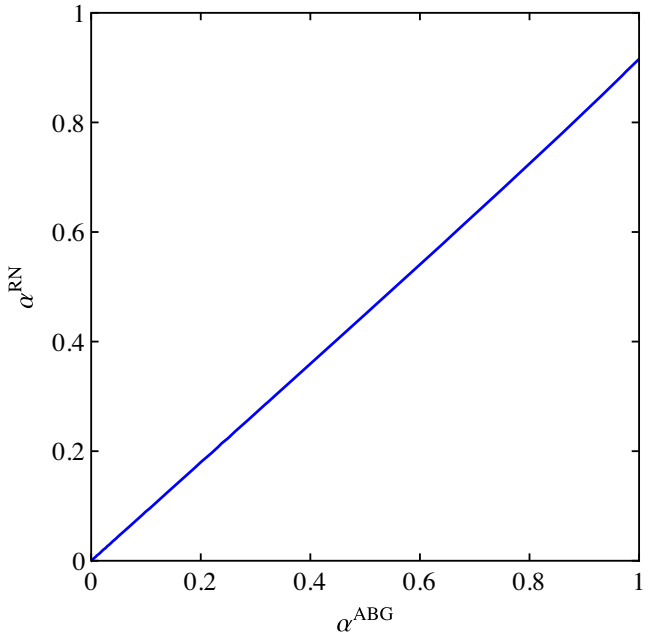

FIG. 14. The values of the normalized charges for which the GCSs of ABG and RN BHs are equal.

VII. FINAL REMARKS

We studied the propagation of a massless and chargeless test scalar field in the background of ABG RBHs, focusing in the absorption process. We computed the ACS numerically and compared our results with limiting cases, showing that they are in excellent agreement.

The metric function and the electric field of ABG RBH tend to the RN BH case in the far-field limit, but close to the event horizon they differ significantly. In particular, the quantities $f^{ABG}(r)$ and $E^{ABG}(r)$ are finite at the origin ($r = 0$), whereas $f^{RN}(r)$ and $E^{RN}(r)$ diverge in this limit. We also note that the magnitude of the event horizon radius, r_+, of both BH solutions is very similar, for the same values of the normalized charge α. The functions $f^{ABG}(r)$ and $f^{RN}(r)$ may be equal at distinct values of r/M.

The GCS for null geodesics of ABG RBH is typically larger than the RN one, as well as r_c and b_c. In the chargeless case ($\alpha = 0$), the GCSs of both ABG and RN BHs are equal to the Schwarzschild result. We obtained that the GCSs of ABG and RN BHs may also be equal for nonvanishing values of the normalized charges, and such an equality can be found for $\alpha^{RN} \lesssim 0.9161$.

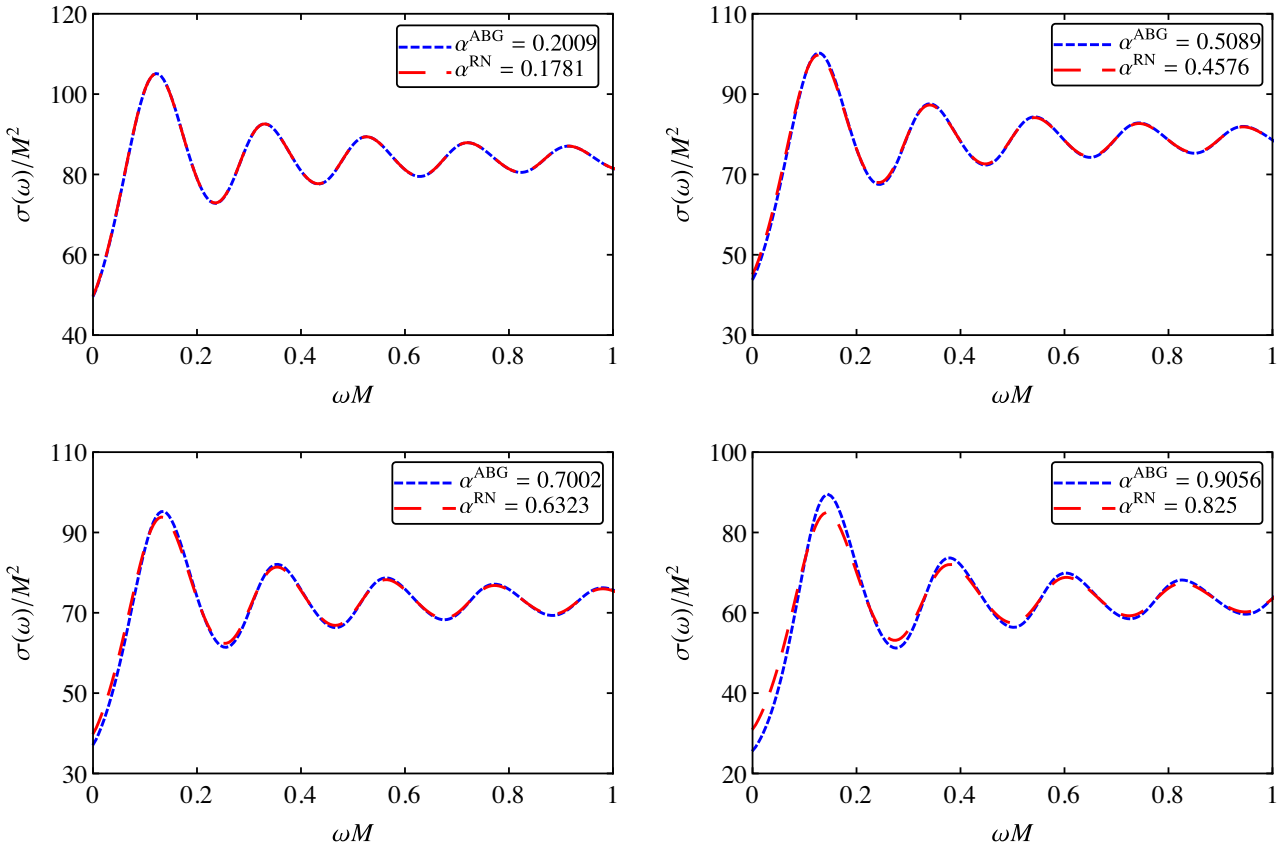

FIG. 15. The total ACSs for some pairs $(\alpha^{ABG}, \alpha^{RN})$ as a function of ω.

The effective potential related to the propagation of massless scalar fields in the background of the ABG RBH presents a peak which increases as we increase l or α. Generically, we note that the total ACS of the ABG RBH, in the mid-to-high frequency limit, oscillates around the corresponding GCS. Besides that, the sinc approximation provides excellent results for the ABG RBH ACS in this regime. We also note that the ABG RBH total ACS diminishes as we increase α. This is in accordance with the fact that $V_{\text{eff}}^{\text{ABG}}(r)$ increases as we increase α, what means that massless scalar waves are subject to higher potential barriers as we consider higher values of α. Moreover, the ABG RBH total ACS is typically larger than the RN one, for the same choice of α.

It was shown in Ref. [38] that the ACSs of the Bardeen RBHs can present an oscillatory behavior similar to those of the RN BHs, in the mid-to-high-frequency regime. Here, we have shown that for small-to-moderate values of the normalized charge, the results for the ACSs of the ABG RBH are very similar to those of the RN BH in the whole frequency range. Hence, from the perspective of the absorption of a nonmassive chargeless test scalar field by a low-charge BH, we may not necessarily distinguish an ABG RBH from a RN BH.

ACKNOWLEDGMENTS

The authors would like to thank C. L. Benone and C. F. B. Macedo for useful discussions. We are grateful to Conselho Nacional de Desenvolvimento Científico e Tecnológico (CNPq) and Coordenação de Aperfeiçoamento de Pessoal de Nível Superior (CAPES)—Finance Code 001, from Brazil, for partial financial support. This research has also received funding from the European Union's Horizon 2020 research and innovation programme under the H2020-MSCA-RISE-2017 Grant No. FunFiCO-777740.

[1] C. M. Will, The Confrontation between general relativity and experiment, Living Rev. Relativity **17**, 4 (2014).
[2] K. Akiyama, A. Alberdi, W. Alef *et al.*, First M87 Event Horizon Telescope Results. I. The shadow of the supermassive black hole, Atrophys. J. **875**, L1 (2019).
[3] B. P. Abbott, R. Abbott, T. D. Abbott *et al.*, Observation of Gravitational Waves from a Binary Black Hole Merger, Phys. Rev. Lett. **116**, 061102 (2016).
[4] M. Heusler, *Black Hole Uniqueness Theorems* (Cambridge University Press, Cambridge, England, 1996).
[5] R. Wald, *General Relativity* (University of Chicago Press, Chicago, 1984).
[6] S. Ansoldi, Spherical black holes with regular center: A review of existing models including a recent realization with Gaussian sources, arXiv:0802.0330.
[7] J. Bardeen, Non-singular general relativistic gravitational collapse, *Proceedings of the International Conference GR5, Tbilisi, U.S.S.R., 1968* (unpublished).
[8] A. Borde, Open and closed universes, initial singularities, and inflation, Phys. Rev. D **50**, 3692 (1994).
[9] C. Barrabès and V. P. Frolov, How many new worlds are inside a black hole? Phys. Rev. D **53**, 3215 (1996).
[10] M. Mars, M. M. Martín-Prats, and J. M. M. Senovilla, Models of regular Schwarzschild black holes satisfying weak energy conditions, Classical Quantum Gravity **13**, L51 (1996).
[11] A. Cabo and E. Ayón-Beato, About black holes with nontrapping interior, Int. J. Mod. Phys. A **14**, 2013 (1999).
[12] E. Ayón-Beato and A. García, Regular Black Hole in General Relativity Coupled to Nonlinear Electrodynamics, Phys. Rev. Lett. **80**, 5056 (1998).
[13] M. Born, On the quantum theory of the electromagnetic field, Proc. R. Soc. A **143**, 410 (1934).
[14] M. Born and L. Infeld, Foundations of the new field theory, Proc. R. Soc. A **144**, 425 (1934).
[15] J. F. Plebański, *Lectures on Non-Linear Electrodynamics* (NORDITA, Copenhagen, Denmark, 1970).
[16] E. S. Fradkin and A. A. Tseytlin, Non-linear electrodynamics from quantized strings, Phys. Lett. B **163**, 123 (1985).
[17] N. Seiberg and E. Witten, String theory and noncommutative geometry, J. High Energy Phys. 09 (1999) 032.
[18] A. A. Tseytlin, Born-Infeld action, supersymmetry and string theory, *The Many Faces of the Superworld* (World Scientific, Singapore, 2000), pp. 417–452.
[19] E. Ayón-Beato and A. García, Non-singular charged black hole solution for non-linear source, Gen. Relativ. Gravit. **31**, 629 (1999).
[20] E. Ayón-Beato and A. García, New regular black hole solution from nonlinear electrodynamics, Phys. Lett. B **464**, 25 (1999).
[21] I. Dymnikova, Regular electrically charged vacuum structures with de Sitter centre in nonlinear electrodynamics coupled to general relativity, Classical Quantum Gravity **21**, 4417 (2004).
[22] L. Balart and E. C. Vagenas, Regular black holes with a nonlinear electrodynamics source, Phys. Rev. D **90**, 124045 (2014).
[23] M. E. Rodrigues and M. V. de S. Silva, Bardeen regular black hole with an electric source, J. Cosmol. Astropart. Phys. 06 (2018) 025.
[24] E. Ayón-Beato and A. García, The Bardeen model as a nonlinear magnetic monopole, Phys. Lett. B **493**, 149 (2000).
[25] K. A. Bronnikov, Regular magnetic black holes and monopoles from nonlinear electrodynamics, Phys. Rev. D **63**, 044005 (2001).

[26] J. Matyjasek, Extremal limit of the regular charged black holes in nonlinear electrodynamics, Phys. Rev. D **70**, 047504 (2004).
[27] M. Ma, Magnetically charged regular black hole in a model of nonlinear electrodynamics, Ann. Phys. (Amsterdam) (N. Y.) **362**, 529 (2015).
[28] S. I. Kruglov, Black hole as a magnetic monopole within exponential nonlinear electrodynamics, Ann. Phys. (Amsterdam) (N. Y.) **378**, 59 (2017).
[29] E. L. B. Junior, M. E. Rodrigues, and M. J. S. Houndjo, Regular black holes in $f(T)$ Gravity through a nonlinear electrodynamics source, J. Cosmol. Astropart. Phys. 10 (2015) 060.
[30] M. V. de S. Silva and M. E. Rodrigues, Regular black holes in $f(G)$ gravity, Eur. Phys. J. C **78**, 638 (2018).
[31] R. Narayan, Black holes in astrophysics, New J. Phys. **7**, 199 (2005).
[32] J. A. Futterman, F. A. Handler, and R. A. Matzner, *Scattering from Black Holes* (Cambridge University Press, Cambridge, England, 1988).
[33] E. S. Oliveira, L. C. B. Crispino, and A. Higuchi, Equality between gravitational and electromagnetic absorption cross sections of extreme Reissner-Nordstrom black holes, Phys. Rev. D **84**, 084048 (2011).
[34] L. C. B. Crispino, S. R. Dolan, A. Higuchi, and E. S. de Oliveira, Inferring black hole charge from backscattered electromagnetic radiation, Phys. Rev. D **90**, 064027 (2014).
[35] L. C. B. Crispino, S. R. Dolan, A. Higuchi, and E. S. de Oliveira, Scattering from charged black holes and supergravity, Phys. Rev. D **92**, 084056 (2015).
[36] C. L. Benone and L. C. B. Crispino, Superradiance in static black hole spacetimes, Phys. Rev. D **93**, 024028 (2016).
[37] L. C. S. Leite, C. L. Benone, and L. C. B. Crispino, Scalar absorption by charged rotating black holes, Phys. Rev. D **96**, 044043 (2017).
[38] C. F. B. Macedo and L. C. B. Crispino, Absorption of planar massless scalar waves by Bardeen regular black holes, Phys. Rev. D **90**, 064001 (2014).
[39] C. F. B. Macedo, E. S. de Oliveira, and L. C. B. Crispino, Scattering by regular black holes: Planar massless scalar waves impinging upon a bardeen black hole, Phys. Rev. D **92**, 024012 (2015).
[40] P. A. Sanchez, N. Bretón, and S. E. P. Bergliaffa, Scattering and absorption of massless scalar waves by Born-Infeld black holes, Ann. Phys. (N.Y.) **393**, 107 (2017).
[41] S. Fernando, Bardeen-de Sitter black holes, Int. J. Mod. Phys. D **26**, 1750071 (2017).
[42] E. Jung and D. K. Park, Absorption and emission spectra of an higher-dimensional Reissner-Nordström black hole, Nucl. Phys. **B717**, 272 (2005).
[43] L. C. B. Crispino, S. R. Dolan, and E. S. Oliveira, Scattering of massless scalar waves by Reissner-Nordström black holes, Phys. Rev. D **79**, 064022 (2009).
[44] H. Salazar, A. García, and J. Plebański, Duality rotations and type D solutions to Einstein equations with nonlinear electromagnetic sources, J. Math. Phys. (N.Y.) **28**, 2171 (1987).
[45] W. Unruh, Absorption cross section of small black holes, Phys. Rev. D **14**, 3251 (1976).
[46] S. R. Das, G. Gibbons, and S. D. Mathur, Universality of Low Energy Absorption Cross Sections for Black Holes, Phys. Rev. Lett. **78**, 417 (1997).
[47] A. Higuchi, Low-frequency scalar absorption cross sections for stationary black holes, Classical Quantum Gravity **18**, L139 (2001); **19**, 599(A) (2002).
[48] N. Sanchez, Absorption and emission spectra of a Schwarzschild black hole, Phys. Rev. D **18**, 1030 (1978).
[49] Y. Décani, G. Esposito-Farèse, and A. Folacci, Universality of high-energy absorption cross sections for black holes, Phys. Rev. D **83**, 044032 (2011).
[50] V. Cardoso, A. S. Miranda, E. Berti, H. Witek, and V. T. Zanchin, Geodesic stability, Lyapunov exponents, and quasinormal modes, Phys. Rev. D **79**, 064016 (2009).